ARTICLE

Biocompatible Interface Films Deposited within Porous Polymers by Atomic Layer Deposition (ALD)

Xinhua Liang, Aaron D. Lynn, David M. King, Stephanie J. Bryant, and Alan W. Weimer*

Department of Chemical and Biological Engineering, University of Colorado, Boulder, Colorado 80309

ABSTRACT Ultrathin ceramic films were deposited throughout highly porous poly(styrene−divinylbenzene) (PS-DVB) particles using a low-temperature atomic layer deposition (ALD) process. Alumina and titania films were deposited by alternating reactions of trimethylaluminum and H_2O at 33 °C and of titanium tetrachloride and H_2O_2 (50 wt % in H_2O) at 100 °C, respectively. Analytical characterization revealed that conformal alumina and titania films were grown on internal and external polymer surfaces. The improved bioactivity of the polymer substrates was revealed on the basis of the formation of hydroxyapatite (HA) in simulated body fluid. The accelerated formation of HA on the ALD-modified polymer surface was caused by the negatively charged surface provided by the ultrathin ceramic interface. The potential for ALD films to support cell attachment was demonstrated.

KEYWORDS: interface film • ceramic • polymer • atomic layer deposition (ALD) • hydroxyapatite (HA) • cell adhesion

1. INTRODUCTION

Porous polymers have attracted increased interest in the field of tissue engineering (1−3), and they can provide three-dimensional structures as scaffolds to guide cell growth and tissue development to replace diseased or damaged tissues resulting from traumas, congenital defects, or other diseases. The ability for a cell to attach and migrate on a substrate or scaffold surface is an important property for tissue engineering (4, 5). However, synthetic polymers tend to have poor mechanical properties for tissues such as bone and typically lack cell-recognition signals, which result in insufficient cell adhesion and proliferation (4). In bone tissue engineering, the interaction between the cells and the scaffold is particularly important to promote osseointegration for creating new bone in the scaffold and integrating with the host bone (6). Hydroxyapatite (HA), due to its biocompatibility and structural similarity to bone mineral, has been successfully used as bone filler (7), coating of orthopaedic implants (8), and filler of inorganic/polymer composites (9) to facilitate osseointegration at the implant surface. The inclusion of the HA phase in the polymer substrates can enhance the bioactivity and subsequent tissue interaction. However, it is difficult to directly deposit or grow one layer of HA on the porous polymer substrate. Ceramics, such as alumina and titania, have been shown to be highly biocompatible with excellent bone bonding properties (10, 11), and titania has been shown to accelerate the formation of HA (12). A novel process to provide a bioactive interface between polymer substrates and an HA layer is to coat the surface of the porous polymer substrate with ultrathin ceramic films while maintaining the original structure and geometric properties of the substrate. Recently, we have successfully coated ultrathin alumina films on highly porous poly(styrene−divinylbenzene) (PS-DVB) particles by atomic layer deposition (ALD) (13).

ALD is a surface-controlled layer-by-layer process (14, 15) that is particularly well-suited for depositing ultrathin and conformal films onto porous substrates (13, 16). The films grown by ALD are inherently controlled by self-limiting sequential surface chemical reactions. The advantages of ALD methods include low processing temperature, independence of line of sight, low impurity content, and pinhole-free deposition. As a result, ultrathin films can be uniformly formed along the surface of the pores. Alumina ALD films can be obtained by the alternating reactions of trimethylaluminum (TMA) and H_2O (17−20). Titania ALD can be synthesized from alternating reactions of titanium tetraisopropoxide (TTIP) and H_2O or H_2O_2 (21−24) or titanium tetrachloride ($TiCl_4$) and H_2O or H_2O_2 (25, 26). The growth rate of the TiO_2 film from $TiCl_4$ is much higher than that from TTIP, due to the steric hindrance between the large TTIP molecules (23), which decreases the concentration of surface reactive sites. In general, H_2O_2 has a higher reactivity than H_2O. The reaction using H_2O_2 is more thermodynamically favorable than that which uses H_2O (21).

The objective for this study was to demonstrate the feasibility of improving the bioactivity of polymer substrate by coating an ultrathin interface film via ALD. As a proof of concept, highly porous PS-DVB particles were employed. Specifically, ultrathin alumina and titania films were deposited throughout both the internal and external surfaces of highly porous polymer particles by ALD in a scalable fluidized bed reactor. The ALD films were characterized by transmission electron microscopy (TEM) and scanning electron microscopy (SEM). The biological properties of the deposited ceramic films were tested by HA formation and cell adhesion.

2. EXPERIMENTAL SECTION

2.1. ALD of Alumina and Titania Films. Highly porous PS-DVB particles were obtained by the copolymerization of styrene

* To whom correspondence should be addressed. E-mail: alan.weimer@colorado.edu.

Received for review May 29, 2009 and accepted August 16, 2009

DOI: 10.1021/am9003667

Published on Web 09/02/2009

and divinylbenzene (13). The particles had a porosity of 85%, a pore volume of 8−10 cm^3/g, a surface area of 43.5 m^2/g, an average pore size of 200 nm, and a density of 70 kg/m^3 (13). A fluidized bed reactor was used to deposit alumina and titania films on the highly porous PS-DVB particles. The system was operated at reduced pressures. Deionized H_2O and TMA (97%, Sigma Aldrich) were used as reactants for Al_2O_3 ALD at a reaction temperature of 33 °C. Concentrated H_2O_2 (50 wt % in H_2O) and $TiCl_4$ (99%, Alfa Aesar) were used as reactants for TiO_2 ALD at a reaction temperature of 100 °C. High-purity N_2 was used as the purge gas to remove any byproducts formed during the reaction and the unreacted precursor. For TiO_2 ALD, a trap containing sodium bicarbonate powders (Fisher Science Education) was connected to the inlet of the vacuum pump to absorb HCl byproduct.

For a typical run, ~4 g of porous particles was loaded into the reactor. The minimum pressure inside the reactor was ~10 Pa. The minimum fluidization superficial gas velocity was 0.8 cm/s. Precursors were fed separately through the distributor plate at the base of the reactor using the driving force of their room-temperature vapor pressures. The flow rates of precursors were adjusted manually using needle valves to ensure that the precursor pressure (~400 Pa) was high enough for particle fluidization. A typical coating cycle used the following sequence: precursor A dose, N_2 purge, evacuation; precursor B dose, N_2 purge, evacuation. A detailed description of the experimental procedure for ALD coating of polymer particles has been published elsewhere (13).

2.2. ALD Film Characterization. The coated samples were analyzed using a JEOL 2010F 200 kV Schottky field emission transmission electron microscope operating in the scanning transmission electron microscopy (STEM, Z-contrast) mode with an electron probe size of 0.2 nm. TEM samples were prepared by placing the crushed porous particles on holey-carbon films supported on Cu grids. The cross-sectioned alumina- and titania-coated porous particles were investigated using a JEOL JSM-7401F field emission scanning electron microscope (FESEM) equipped with an EDAXS detector unit for elemental analysis while imaging. Specimens were prepared by cutting the coated particles using a Super Gillette blue blade. At least three spots of two different particles were analyzed per sample for TEM and FESEM analysis.

2.3. Hydroxyapatite Formation. In vitro bioactivity studies of the composite particles were assessed by immersion in simulated body fluid (SBF) for different periods of time. The uncoated and alumina (25 cycles) and titania (50 cycles) ALD surface modified PS-DVB particles were incubated in SBF at 37 °C. The SBF was prepared by dissolving reagent grade NaCl, $NaHCO_3$, KCl, $K_2HPO_4 \cdot 3H_2O$, $MgCl_2 \cdot 6H_2O$, $CaCl_2$, and Na_2SO_4 in deionized water and buffering at a pH value of 7.3 with tris(hydroxymethyl)aminomethane ($(CH_2OH)_3CNH_2$) and hydrochloric acid (HCl) (27). All of the aforementioned chemicals were obtained from Sigma Aldrich. The ion concentrations were nearly equal to those of human blood plasma (27). The SBF solution was changed every 2−3 days. After incubation at 37 °C for different periods of time, polymer particles were removed from the SBF, rinsed gently with deionized water twice, and vacuum-dried overnight. There is one duplicate run for some of the HA formation experiments. At least three spots of two particles of each sample were analyzed by FESEM and EDS to verify the deposition of HA on the particle surface. Powder X-ray diffraction (XRD) spectra were obtained using an Inel CPS 120 diffraction system (Cu Kα radiation).

2.4. Cell Adhesion. The uncoated and alumina- and titania-coated porous particles were soaked in cell growth media for 3 days (two media changes per day) prior to exposing to a cell suspension of NIH/3T3 fibroblast cells to remove the possible cytotoxic byproducts, such as trace residue of HCl on titania ALD films. Using a six-well culture dish, approximately 45 mg of particles was placed into each well with 3 mL of cell growth media with 3.3×10^5 cells/mL. The cell suspensions were incubated at 37 °C for 3 h, the media was aspirated, and particles were washed gently two times in phosphate-buffered saline (PBS). Live cells attached to the particles were visualized by a live cell cytoplasmic stain, Calcein AM (Molecular Probes), at a concentration of 2 μmol/L in PBS for 30 min at 37 °C. Particles were gently rinsed two times with PBS and imaged using laser scanning confocal microscopy (Zeiss, LSM5 Pascal).

3. RESULTS AND DISCUSSION

3.1. Conformal ALD Coatings. The alumina- and titania-coated porous polymer particles were analyzed using

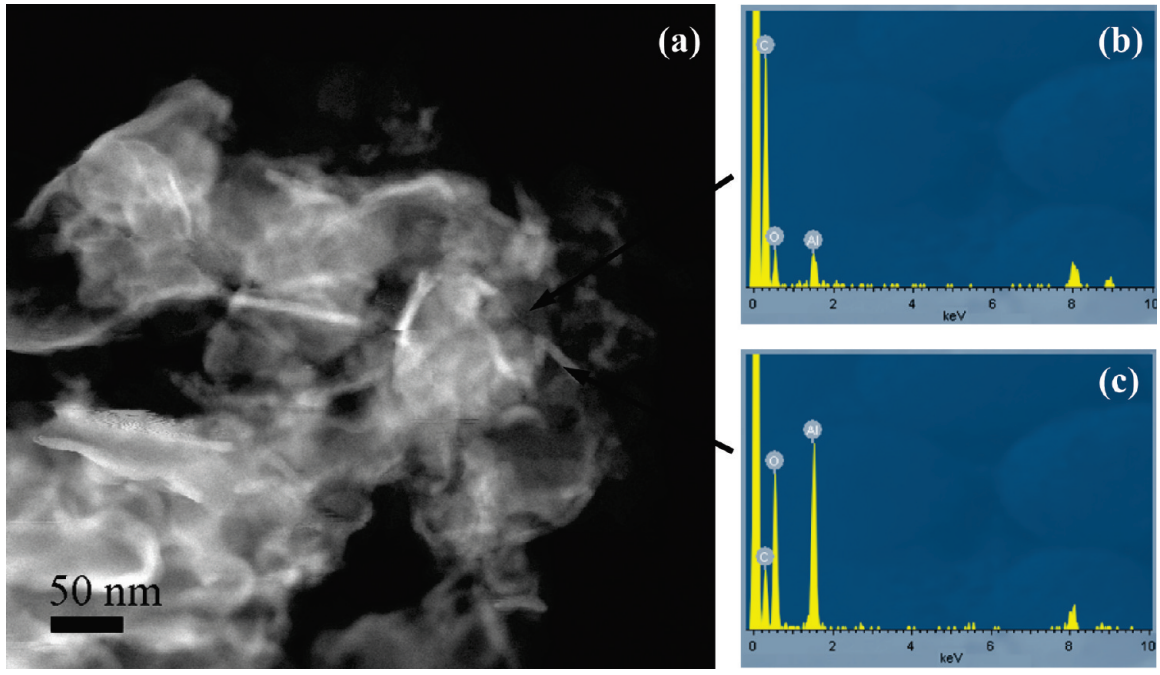

FIGURE 1. (a) Z-contrast image of crushed Al_2O_3-coated porous polymer particles after 25 cycles and EDS spectra of (b) the polymer substrate and (c) the Al_2O_3 ALD film.

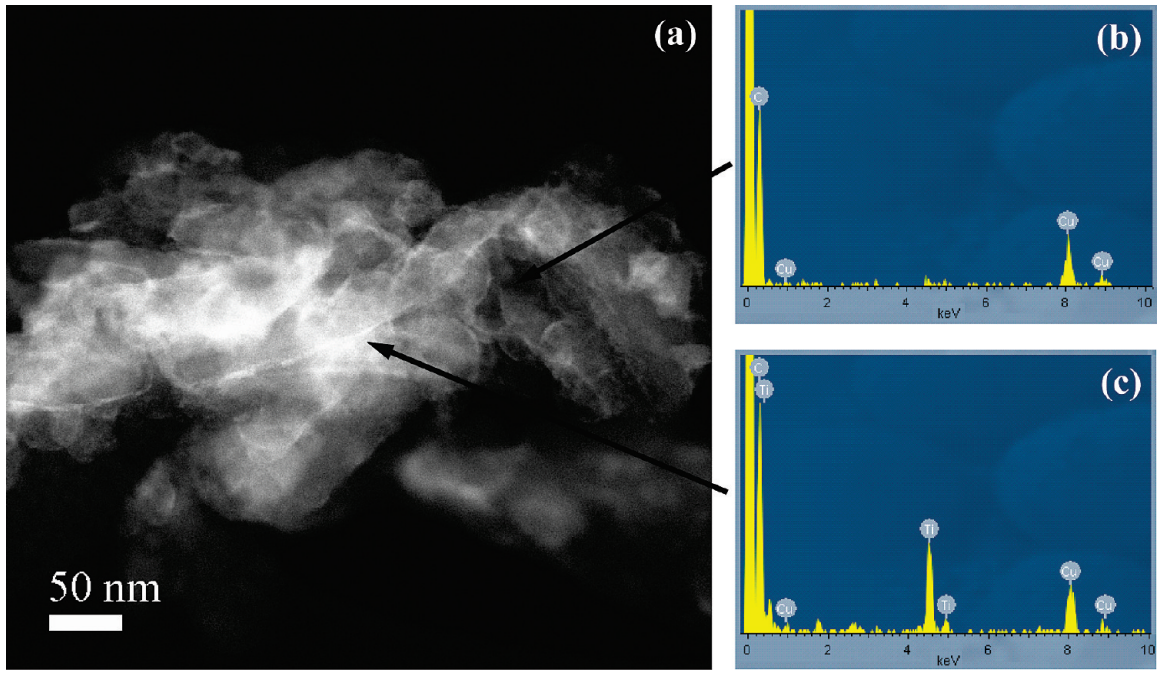

FIGURE 2. (a) Z-contrast image of crushed TiO_2-coated porous polymer particles after 50 cycles and EDS spectra of (b) the polymer substrate and (c) the TiO_2 ALD film.

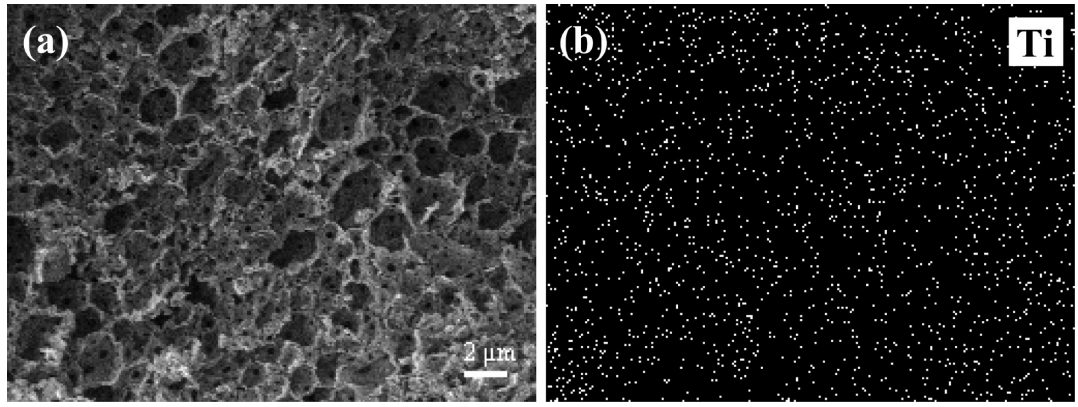

FIGURE 3. Cross-sectional FESEM and EDS images of a TiO_2-coated porous polymer particle: (a) FESEM image of cross-sectioned surface of a TiO_2-coated porous polymer particle after 50 cycles and (b) titanium EDS signal of the same cross-sectioned surface.

atomic resolution Z-contrast imaging. Because of the difference in the atomic weight of the ALD films and polymer, Z-contrast imaging is ideal to observe the degree and quality of ALD films deposited on polymer surfaces. A representative Z-contrast image of the alumina-coated polymer particles after 25 coating cycles is shown in Figure 1. The regions with a brighter contrast (i.e., regions with heavier Z) in Figure 1a were determined to be mostly alumina by elemental nanoanalysis using energy dispersive spectrometry (EDS), as shown in Figure 1b,c. The alumina films appeared to be uniform and smooth. On the basis of STEM images, the thickness of the alumina films was ~8 nm, which represented a growth rate of ~0.3 nm per coating cycle under the experimental conditions. These results were consistent with those previously obtained (13). A representative Z-contrast image of the titania-coated polymer particles after 50 coating cycles is shown, along with the respective EDS plots, in Figure 2. The titania films also exhibited the smoothness and uniformity characteristic of ALD processes. On the basis of STEM images, the thickness of the titania films was ~3 nm, which represented a growth rate of ~0.06 nm per coating cycle and compared well with literature values (25). The STEM images confirmed the presence of the conformal ceramic films throughout the porous structure, which indicated that ceramic films could be grown on the internal and external polymer particle surfaces using this gas-phase deposition technique.

The deposition of alumina and titania films inside the porous network was further investigated using the FESEM with EDS measurements on cross-sectioned samples. The presence of titanium throughout the inner surface of the porous particles was verified by tracking the titanium EDS mapping signal, shown in Figure 3. An aluminum EDS mapping signal also illustrated the presence of aluminum throughout the cross-sectioned alumina coated porous polymer sample (data not shown). Therefore, the precursors that were used for alumina and titania film growth were able to infiltrate the porous network to allow for the facile formation

of chemisorbed ceramic materials, distributed homogeneously across the polymer surfaces.

Alumina and titania ALD on this porous polymer resulted in conformal coatings on the pore walls, since ALD reaction is self-limiting and self-terminating, and the growth rate is a constant per AB cycle (13). The ultrathin alumina or titania films can provide for modifying the surface properties of porous polymer while keeping its porous structure property unchanged. On the basis of the Brunauer–Emmett–Teller (BET) surface area measurement, the surface area of the alumina-coated particles decreased with the increasing ALD coating cycles. For example, the particle surface area was 19.4 m^2/g after 25 cycles (43.5 m^2/g for uncoated sample) (13), which means some nanoscale pores (< 15 nm) were inaccessible with the increasing coating cycles.

3.2. Hydroxyapatite Formation. To examine the ability of the ceramic-coated polymers to nucleate and deposit HA on the material surface in vitro, the uncoated and the ceramic-coated samples were soaked in SBF for different periods of time. This process is known in the literature as a "biomimetic process" (28). The samples were characterized after immersion in SBF for 1–2 weeks. FESEM examination of all tested samples indicated changes in the appearance and morphology (microstructure) of the materials after incubation in SBF. Figure 4 shows the FESEM images of the Al_2O_3-coated porous polymer samples before and after incubation in SBF at 37 °C. In comparison to Figure 4a, after 1 week, the surface of the polymer substrate was roughened and several small, individual HA particles (Figure 4b) were formed. After 2 weeks (Figure 4c), the amount of HA present on the substrate surface was greatly increased. Moreover, nanoscale HA particles were homogeneously dispersed and formed a fairly dense coating on the substrate surface. The substrate surface appeared considerably rougher compared to the surface before HA formation. In order to verify the composition of the HA, EDS was performed to analyze the composition of the particular matter formed on the substrate surface. The EDS spectrum (Figure 4d) confirmed that a considerable amount of calcium (Ca) and phosphorus (P) was present on the roughened surface, in relative amounts that are typical of HA compositions.

Figure 5 shows the FESEM images of the TiO_2-coated polymer substrate surfaces before and after incubation in SBF at 37 °C. In comparison to Figure 5a, after 1 week, the surface of the polymer became rough and some small particles were formed, which again indicated the formation of HA. After 2 weeks (Figure 5c), the amount of HA greatly increased. The homogeneous distribution of nanoscale HA particles can be seen in Figure 5c. Similar to the Al_2O_3-coated case, the EDS spectrum of the TiO_2-coated surface (Figure 5d) confirmed the presence of a considerable amount of Ca and P. The trace amount of chlorine (Cl) present was due to the residue from the low-temperature TiO_2 ALD process. The grain size of HA formed on the TiO_2-coated porous polymer surface was much larger than the size of those formed on the Al_2O_3-coated polymer surface, which may suggest that

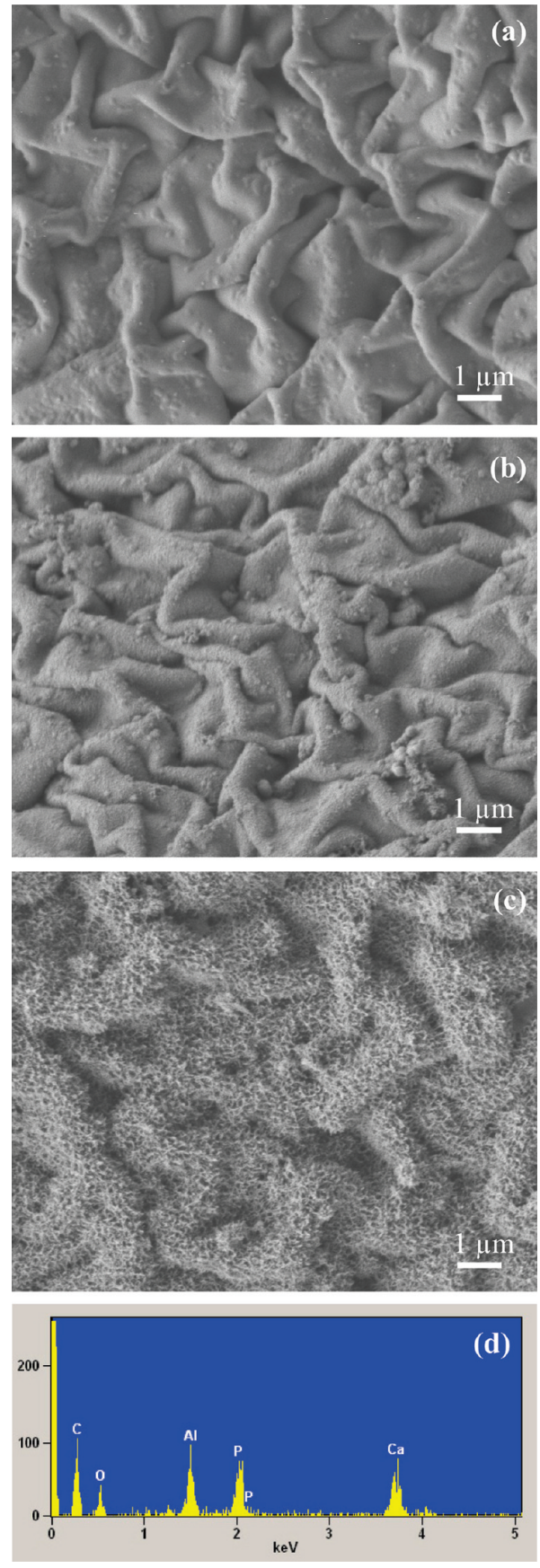

FIGURE 4. FESEM images of an alumina-coated polymer particle (a) before and (b, c) after incubation in SBF at 37 °C for (b) 1 week and (c) 2 weeks and (d) EDS spectrum of an alumina-coated polymer particle after incubation in SBF for 2 weeks.

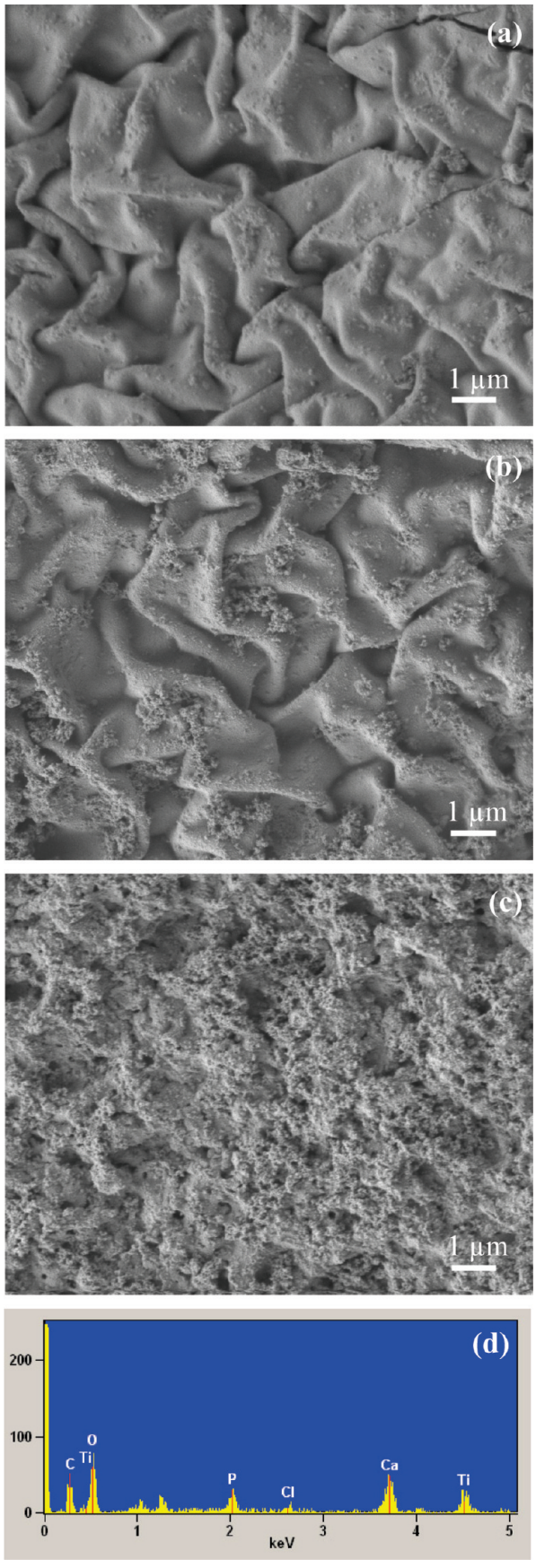

FIGURE 5. FESEM images of a titania-coated polymer particle (a) before and (b, c) after incubation in SBF at 37 °C for (b) 1 week and (c) 2 weeks and (d) EDS spectrum of a titania-coated polymer particle after incubation in SBF for 2 weeks.

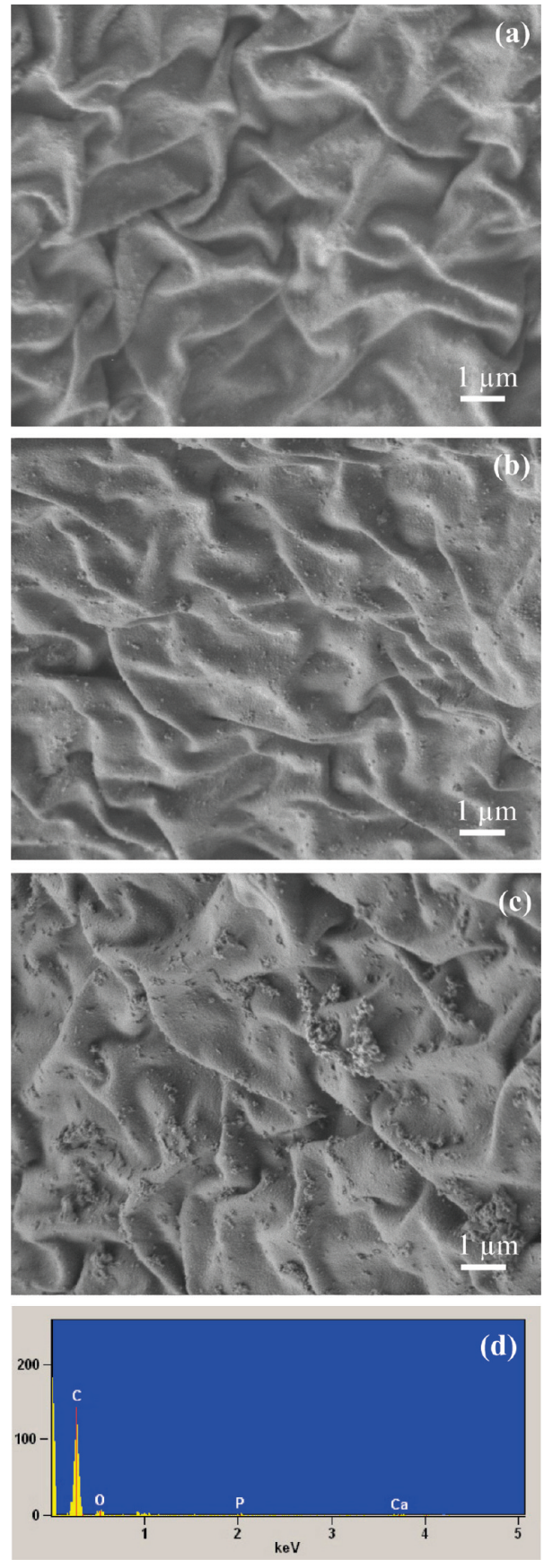

FIGURE 6. FESEM images of an uncoated porous polymer particle (a) before and (b, c) after incubation in SBF at 37 °C for (b) 1 week and (c) 2 weeks and (d) EDS spectrum of an uncoated porous polymer particle after incubation in SBF for 2 weeks.

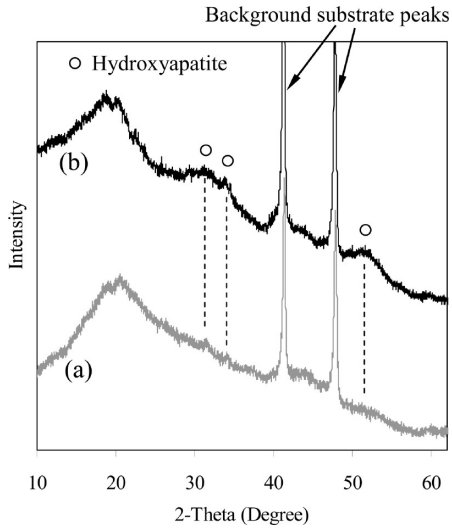

FIGURE 7. XRD spectra of (a) uncoated and (b) 25 cycle alumina-coated PS-DVB particles after incubation in SBF at 37 °C for 2 weeks.

the growth rate of HA on TiO_2 films could proceed much faster. However, the reason for this higher growth rate is not clear.

For comparison, the FESEM images of uncoated polymer before and after incubation in SBF at 37 °C are shown in Figure 6. In comparison to the FESEM image of the polymer surface before incubation in SBF (Figure 6a), Figure 6b,c revealed some evidence of HA formation over the incubation time, but a homogeneous distribution of HA was not observed. This observation was confirmed by EDS analysis (Figure 6d) of the composition of the polymer surface after incubation in SBF for 2 weeks, but there was only a trace amount of Ca and P present. Ultimately, these results confirmed that the uncoated polymer could achieve only low HA growth rates. Hence, it is particularly compelling that biocompatible surfaces can be formed on PS-DVB with Al_2O_3 and TiO_2 ALD films. Such coatings are particularly attractive for use with more conventionally used porous biocompatible polymers.

Figure 7 shows powder XRD patterns of the uncoated and alumina-coated (25 cycles) PS-DVB samples after incubation in SBF solution for 2 weeks. The XRD patterns further verified that the films formed on polymer substrate surfaces were HA. The XRD signal of the HA formed on the alumina-coated particle surface was stronger than that of the HA formed on the uncoated particle surface, especially for the peak at 51.6°, which corroborated the results observed from FESEM and EDS.

Theoretically, as long as the pores in the polymer substrate are larger than the diameter of the ions in the solution, the ions can diffuse into the pores and form a layer of HA, as was observed on the polymer surfaces. To ensure the formation of HA inside the porous structure, as well as the distribution and morphology of adhered HA, cross-sectioned alumina-coated particles were characterized by FESEM and EDS measurements. As shown in Figure 8, the phosphorus and calcium EDS mapping signal illustrated the presence of HA throughout the inner surface of the porous polymer. Therefore, HA was formed not only on the outside surface of the porous polymer but also throughout the inside of the pores of the porous polymer.

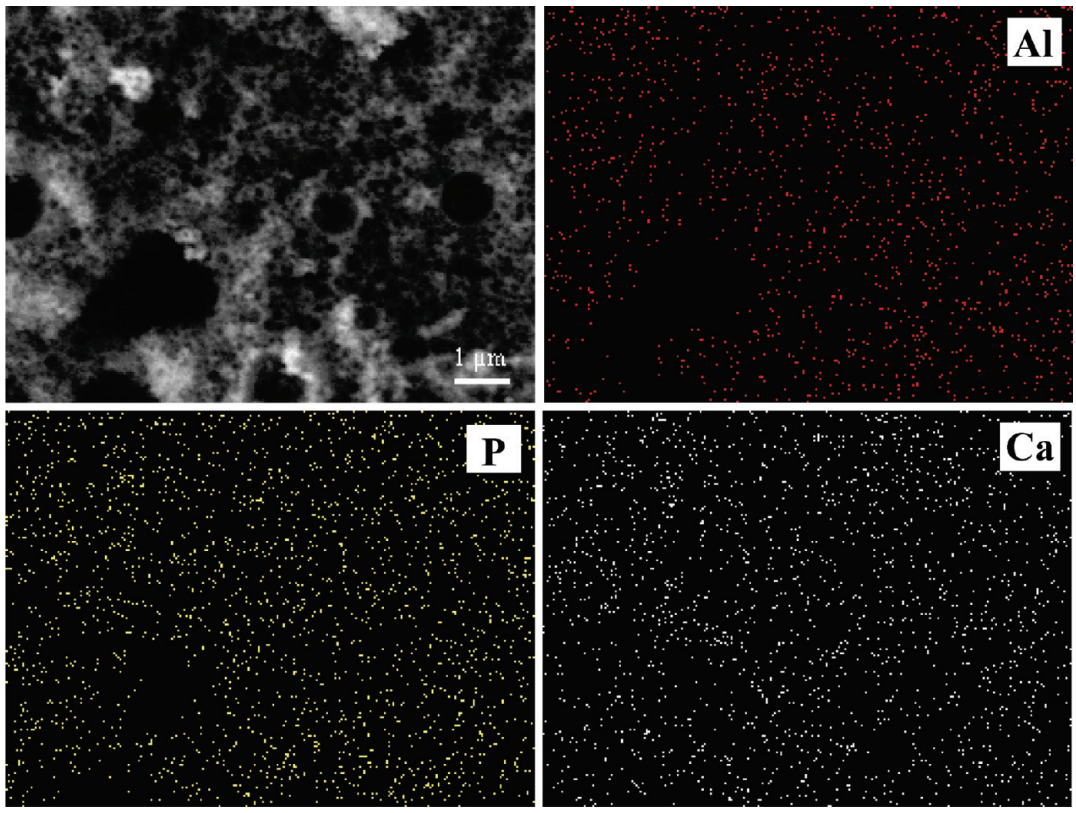

FIGURE 8. FESEM image of cross-sectioned surface of an alumina-coated polymer particle after incubation in SBF at 37 °C for 2 weeks and Al, P, and Ca EDS signals of the same cross-sectioned surface.

This set of experiments indicated that the deposition of ultrathin (~3−8 nm) alumina and titania ALD films can efficiently promote the formation of HA in SBF. The formation mechanism of HA on the surface of different substrates has been examined by different research groups. Li et al. proposed the "charged surface" theory and hypothesized that the hydroxyl groups on the surface, which caused the surface to be negatively charged, were critical for HA nucleation on the surfaces in SBF (12). Takadama et al. investigated the mechanism of biomineralization of HA on sodium silicate glass using TEM-EDX and also proposed that the formation of HA on the surface of sodium silicate glass was mainly attributed to the charged surface (29, 30). The formation of a negatively charged surface is generally regarded to be important to allow for the precipitation of HA in SBF.

Both Al_2O_3 and TiO_2 are able to absorb water at the surface, resulting in aluminum hydroxide (Al−OH) and titanium hydroxide (Ti−OH) groups. In the buffered and neutral supersaturated SBF solution (pH 7.3), both Al−OH and Ti−OH groups dissociate, leading to a negatively charged surface that provides sites for calcium phosphate nucleation. The calcium ions in the SBF solution are attracted to the negatively charged surface site, and subsequently the arrival of HPO_4^{2-} results in a hydrated precursor cluster consisting of calcium hydrogen phosphate. After the precursor clusters are formed, they spontaneously grow by consuming calcium and phosphate ions from the surrounding body fluid. The significant increase in HA formation on the ALD-coated polymer surface indicated the improved bioactivity of the substrate relative to the uncoated case.

3.3. Cell Adhesion on Porous Particles. The potential of the uncoated and ceramic-coated porous particles to promote cell attachment and spreading was assessed using a model cell, NIH/3T3 fibroblasts. Particles were washed multiple times to remove the potential cytotoxic byproducts before the test. Figure 9a shows NIH/3T3 cell attachment to the surface of an alumina-coated porous particle after 3 h. A small degree of cell spreading along the surface of the particle was observed. The cell morphology was similar to that of cells seeded onto tissue culture treated polystyrene and cultured for 3 h (data not shown). Figure 9b shows a section from a Z-stack through an alumina-coated particle (10 μm thick) to illustrate the cell presence and morphology at the outer surface of the particle. Due to the small pore size of the particles, cells were only present on the surface of the particles. Similar cell densities and morphologies were seen on both the uncoated and titania-coated porous polymers (data not shown), indicating that ALD ceramic film surfaces promote cellular attachment and growth. Though both uncoated and ceramic-coated porous particles supported cell attachment and spreading, the ability to create surfaces that both promote cell adhesion and HA formation is attractive for designing a biomaterial for bone regeneration, which is only observed in the ceramic-coated substrates.

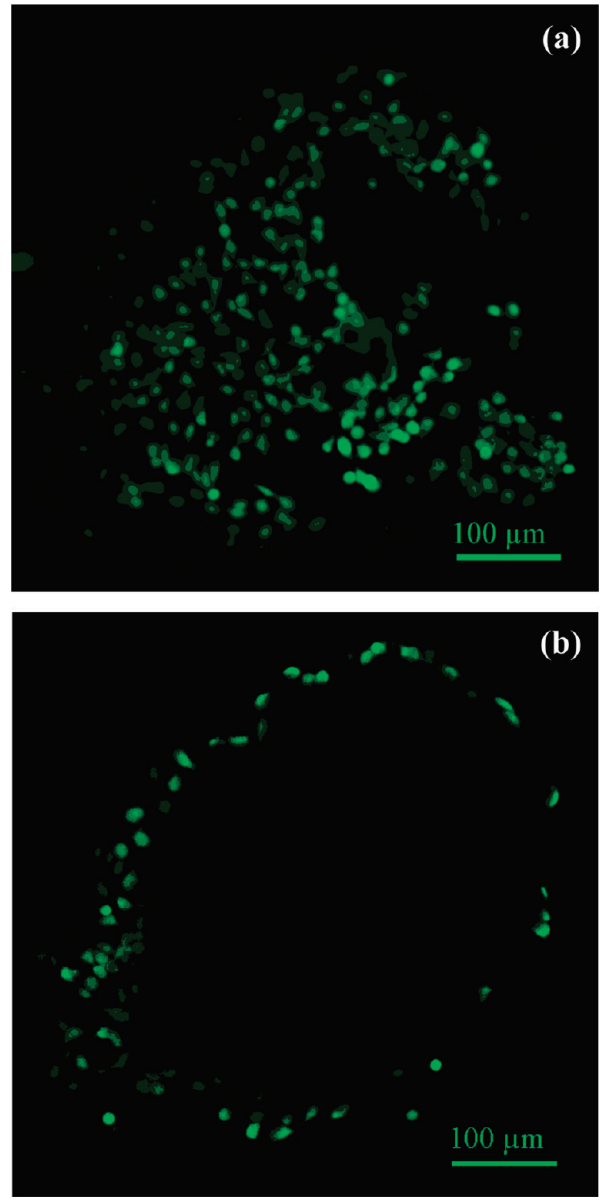

FIGURE 9. Fluorescent confocal laser scanning microscopy images of (a) NIH/3T3 fibroblasts (green) adhered to an alumina-coated porous polymer particle after 3 h and (b) a 10 μm slice through an alumina-coated porous polymer particle illustrating fibroblast adhesion to the particle surface. Cell cytosol was stained with Calcein AM.

4. CONCLUSIONS

Ultrathin alumina and titania films were deposited throughout highly porous PS-DVB particles by ALD in a fluidized bed reactor at low temperatures. Analytical characterization revealed that conformal alumina and titania films were grown on the internal and external polymer particle surfaces. The improved bioactivity of the polymer substrates was revealed on the basis of the formation of hydroxyapatite in SBF, which was confirmed by FESEM-EDS. The accelerated formation of HA on the ALD-modified polymer surface was caused by the negatively charged surface provided by the ultrathin ceramic interface. The potential for ALD films to support cell attachment was demonstrated. However, additional studies are necessary to assess the biocompatibility of the ALD films.

The impetus behind this study was to demonstrate a convenient and universal surface treatment strategy for modifying the surface properties of porous polymer materials and thus a method to promote the bioactivity and cell adhesion of the polymer substrate. Surface modification of porous polymers with ultrathin ceramic ALD films provides a new class of polymer/ceramic composite materials with potentially greater material strength and enhanced bioactivity for tissue regeneration. Future work will focus on the deposition of ceramic films on more appropriate porous scaffolds which are being used in bone tissue engineering, such as poly(lactic acid), poly(lactide-co-glycolide) and poly(2-hydroxyethyl methacrylate).

Acknowledgment. This work was partially supported by the National Science Foundation under Grant No. 0400292. Any opinions, findings, and conclusions or recommendations expressed in this work are those of the authors and do not necessarily reflect the views of the National Science Foundation. We thank Dr. Peng Li for the STEM analysis and Dr. Yanfeng Zhang for the XRD analysis.

REFERENCES AND NOTES

(1) Wang, X. X.; Li, W.; Kumar, V. *Biomaterials* **2006**, *27*, 1924–1929.
(2) Macintyre, F. S.; Sherrington, D. C.; Tetley, L. *Macromolecules* **2006**, *39*, 5381–5384.
(3) Boccaccini, A. R.; Maquet, V. *Compos. Sci. Technol.* **2003**, *63*, 2417–2429.
(4) Hu, K.; Lv, Q.; Cui, F. Z.; Xu, L.; Jiao, Y. P.; Wang, Y.; Feng, Q. L.; Wang, H. L.; Huang, L. Y. *J. Bioact. Compat. Polym.* **2007**, *22*, 395–410.
(5) Lu, Q. J.; Ganesan, K.; Simionescu, D. T.; Vyavahare, N. R. *Biomaterials* **2004**, *25*, 5227–5237.
(6) Morra, M.; Cassinelli, C.; Cascardo, G.; Mazzucco, L.; Borzini, P.; Fini, M.; Giavaresi, G.; Giardino, R. *J. Biomed. Mater. Res., Part A* **2006**, *78A*, 449–458.
(7) Wilson, J.; Low, S. B. *J. Appl. Biomater.* **1992**, *3*, 123–129.
(8) Cheang, P.; Khor, K. A.; Teoh, L. L.; Tam, S. C. *Biomaterials* **1996**, *17*, 1901–1904.
(9) Labella, R.; Braden, M.; Deb, S. *Biomaterials* **1994**, *15*, 1197–1200.
(10) Warashina, H.; Sakano, S.; Kitamura, S.; Yamauchi, K. I.; Yamaguchi, J.; Ishiguro, N.; Hasegawa, Y. *Biomaterials* **2003**, *24*, 3655–3661.
(11) Rezwan, K.; Chen, Q. Z.; Blaker, J. J.; Boccaccini, A. R. *Biomaterials* **2006**, *27*, 3413–3431.
(12) Li, P. J.; Kangasniemi, I.; Degroot, K.; Kokubo, T. *J. Am. Ceram. Soc.* **1994**, *77*, 1307–1312.
(13) Liang, X. H.; George, S. M.; Weimer, A. W.; Li, N. H.; Blackson, J. H.; Harris, J. D.; Li, P. *Chem. Mater.* **2007**, *19*, 5388–5394.
(14) Suntola, T. *Thin Solid Films* **1992**, *216*, 84–89.
(15) George, S. M.; Ott, A. W.; Klaus, J. W. *J. Phys. Chem.* **1996**, *100*, 13121–13131.
(16) Mahurin, S.; Bao, L. L.; Yan, W. F.; Liang, C. D.; Dai, S. *J. Non-Cryst. Solids* **2006**, *352*, 3280–3284.
(17) Hakim, L. F.; Vaughn, C. L.; Dunsheath, H. J.; Carney, C. S.; Liang, X. H.; Li, P.; Weimer, A. W. *Nanotechnology* **2007**, 18 Art. No. 345603.
(18) Liang, X. H.; Hakim, L. F.; Zhan, G. D.; McCormick, J. A.; George, S. M.; Weimer, A. W.; Spencer, J. A.; Buechler, K. J.; Blackson, J.; Wood, C. J.; Dorgan, J. R. *J. Am. Ceram. Soc.* **2007**, *90*, 57–63.
(19) Liang, X. H.; Zhan, G. D.; King, D. M.; McCormick, J. A.; Zhang, J.; George, S. M.; Weimer, A. W. *Diamond Relat. Mater.* **2008**, *17*, 185–189.
(20) Zhan, G. D.; Du, X. H.; King, D. M.; Hakim, L. F.; Liang, X. H.; McCormick, J. A.; Weimer, A. W. *J. Am. Ceram. Soc.* **2008**, *91*, 831–835.
(21) Aarik, J.; Aidla, A.; Uustare, T.; Ritala, M.; Leskela, M. *Appl. Surf. Sci.* **2000**, *161*, 385–395.
(22) King, D. M.; Liang, X. H.; Zhou, Y.; Carney, C. S.; Hakim, L. F.; Li, P.; Weimer, A. W. *Powder Technol.* **2008**, *183*, 356–363.
(23) Ritala, M.; Leskela, M.; Niinisto, L.; Haussalo, P. *Chem. Mater.* **1993**, *5*, 1174–1181.
(24) Liang, X. H.; King, D. M.; Li, P.; Weimer, A. W. *J. Am. Ceram. Soc.* **2009**, *92*, 649–654.
(25) Ferguson, J. D.; Yoder, A. R.; Weimer, A. W.; George, S. M. *Appl. Surf. Sci.* **2004**, *226*, 393–404.
(26) Jogi, I.; Kukli, K.; Aarik, J.; Aidla, A.; Lu, J. *Mater. Sci. Semicond. Process.* **2006**, *9*, 1084–1089.
(27) Ohtsuki, C.; Kokubo, T.; Yamamuro, T. *J. Non-Cryst. Solids* **1992**, *143*, 84–92.
(28) Kokubo, T. *Thermochim. Acta* **1996**, *280*, 479–490.
(29) Takadama, H.; Kim, H. M.; Kokubo, T.; Nakamura, T. *J. Biomed. Mater. Res.* **2001**, *57*, 441–448.
(30) Takadama, H.; Kim, H. M.; Kokubo, T.; Nakamura, T. *Chem. Mater.* **2001**, *13*, 1108–1113.

AM9003667